Impact of Distributed Rooftop Photovoltaic Systems on Short-Circuit Faults in the Supplying Low Voltage Networks

Hadi Hosseinian Yengejeh[1], Farhad Shahnia[2*], and Syed M. Islam[1]

[1] School of Electrical Engineering & Computing, Curtin University, Perth, Australia

[2] School of Engineering & Information Technology, Murdoch University, Perth, Australia

([*] Corresponding Author: f.shahnia@murdoch.edu.au, Tel +61-8-93607429)

***Abstract*—**This paper evaluates the effect of randomly distributed, residential single-phase rooftop photovoltaic systems in the low voltage residential networks, during short-circuit faults on the overhead lines. The important parameters such as the fault current, the current sensed at the distribution transformer secondary, and the voltage profile along the feeder during the fault are examined. A sensitivity analysis is carried out in which the rating and location of the photovoltaic systems in the feeder, as well as the fault location and type, are the considered variables. Moreover, to demonstrate the effect of multiple photovoltaic systems with different ratings and penetration levels when distributed unequally among three phases of the network, a stochastic analysis is carried out. The paper summarizes the outcomes of these two analyses to provide a better understanding of the impact of single-phase rooftop photovoltaic systems on the residential feeders during short-circuit faults.

***Keywords*—**Residential Rooftop single-phase photovoltaic systems, Short-circuit faults, Sensitivity analysis, Stochastic analysis.

Nomenclature

BOF	Beginning of feeder	MVF	Medium voltage feeder
EAV	Expected average voltage	PDF	Probability density function
EOF	End of feeder	PDP	Photovoltaic disconnection probability
FCD	Fault current difference	PPL	Photovoltaic penetration level
LG-F	Line-to-ground fault	PV	Photovoltaic unit
LL-F	Line-to-line fault	SCF	Short-circuit fault
LLG-F	Two-line to ground fault	STD	Standard deviation
LVF	Low voltage feeder	TCD	Transformer current difference
MCA	Monte Carlo analysis	VD	Voltage difference
MOF	Middle of feeder		

1. Introduction

Residential rooftop single-phase photovoltaic units, referred to as 'PVs' in this paper, are the most common type of distributed energy resources in the low voltage feeders (LVFs) of many countries including Australia. In Australia, PVs have been installed by a large percentage of the householders due to the state and federal subsidies [1-2]. The effect of high PV penetration levels (PPLs) in LVFs has been studied from power quality and voltage quality points of view in [3-7]. It has been concluded in these studies that a large PPL may lead to the bi-directional power flow in the LVF, and a change in the fault current and its direction in the network. Currently, a PPL of over 25-30% is not allowed by the Australian utilities in their distribution systems [8]. One of the reasons behind this limit is the unknown effects of high PPL in LVFs during short-circuit faults (SCFs).

The impact of three-phase PV plants, installed in medium voltage feeders (MVFs), are studied from protection aspects in [9] in which the PV plant location in the network and its generation capacity and availability are focused. In [10-12], it is discussed that the presence of three-phase renewable energy resources in MVFs may lead to miscoordination among the protection devices, unwanted tripping, protection blinding, and asynchronous reclosing. It is stated in [9, 13-15] that substantial penetration of three-phase renewable resources needs utilization of bidirectional relays, communication-based transfer trips, pilot signal relaying, and impedance-based protection schemes.

Although the impact of large-scale three-phase PV plants has been studied extensively on the SCFs in the network, such a study is not carried out for LVFs with single-phase PVs that may have different ratings and may be distributed unequally among three phases of the network. Reference [16] has considered the SCFs on the systems in the presence of single-phase PVs; however, it is focused on the SCFs in distribution boxes and does not examine the SCFs on the overhead lines, which are more vulnerable. Reference [17] has investigated the impact of single-phase PVs on the coordination of the overcurrent relays in the MVF. It has been concluded in this research that the location of rooftop PVs may affect the operation time of the overcurrent relays adversely. To the best of the authors' knowledge, no technical report has comprehensively evaluated the impact of rooftop PVs on the voltage profile of the LVFs and the current sensed at the secondary side of the distribution transformers during SCFs on LVFs. This is the research gap that is addressed in this research. The voltage magnitude at the feeder connection point to a PV is a key parameter for the disconnection of PVs after an SCF in the LVF. Similarly, the current sensed at the secondary side of the distribution transformer is a key factor in the operation of the switch-fuse for the protection of the system in case of SCFs in the LVF. Therefore, these two parameters are focused in this research.

The preliminary results of the impact of single-phase PVs on the voltage profile and current sensed at the secondary side of the distribution transformers have been demonstrated by the authors in [18], during line-to-ground faults (LG-Fs) on the

overhead lines of the LVFs. The work presented here is aligned with the research in [18] but is extended to cover the line-to-line faults (LL-Fs) and two-line to ground faults (LLG-Fs), which are the most frequent SCFs in LVFs [19]. The research presents a sensitivity analysis to evaluate the contribution of PVs on the SCF current, current sensed at the secondary of the distribution transformer, as well as the voltage profile along the LVF, during SCFs. The rating and location of the PVs, in addition to the SCF location and type, are considered as the variables of the analysis. The research is then expanded to consider the impact of multiple PVs with different ratings, PPLs and random (unequal) distribution among the three phases of the network. This is carried out with the help of a Monte Carlo analysis (MCA)-based stochastic analysis. The sensitivity and stochastic analyses are performed in MATLAB, and their results are validated by PSCAD/EMTDC simulations. The paper summarizes the outcomes of these two analyses to provide a better understanding of the impact of single-phase rooftop PVs on residential LVFs during SCFs. This is the main contribution of this paper. In summary, this research aims to answer the following questions:

- How strong is the impact of a rooftop PV on the current that is observed at the secondary side of the distribution transformers, during SCFs in the LVF?
- How strong is the impact of a rooftop PV on the voltages of the nodes along the LVF, during SCFs?
- What is the impact of different penetrations and ratings of rooftop PVs on the two above parameters?

The rest of the paper is organized as follows: Section 2 presents the network under consideration and the impact of a PV on the system voltages and currents during an SCF. The modeling of the considered system for SCF studies is introduced in details in Section 3. This Section also discusses the developed sensitivity and stochastic analyses. Section 4 illustrates the sensitivity analysis results for the voltage profile along the LVF as well as the current sensed at the secondary side of the distribution transformer during different types of SCFs. The MCA-based stochastic analysis results of the system, in the presence of multiple PVs, with different ratings, installation points along the LVF, PPL, and numbers in each phase of the system, are provided in Section 5. The results of the analyses are discussed in Section 6 while Section 7 summarizes and highlights the general conclusions and findings of the research.

2. Network under Consideration

Let us consider the 10-node, radial, residential supply system of Fig. 1a which represents a typical practical Australian LVF supplying household loads. In Australia, residential LVFs are mostly three-phase, four-wire, multiple earthed neutral (MEN) systems, and are supplied by three-phase Dyn distribution transformers [20]. The distribution transformers are supplied by three-phase, three-wire MVFs. All houses are assumed as single-phase loads. The LVFs are protected by switch-fuses at the secondary side of the distribution transformer to protect the system in case of SCFs in the LVF. The distribution

transformers are usually in the range of 25 to 630 kVA, and the LVFs are generally 400 meters long, distributed through 10-12 poles, with a distance of 30-40 meters from each other. It is to be noted that although similar systems are common in Europe, Asia, and Africa, its structure and topology is different from the LVFs of the North American countries.

The residential rooftop PVs in Australia are single-phase units (composed of PV cells, inverters, and disconnectors). They have a nominal rating of 1-5 kW (depending on the financial status of the householders). The number of rooftop PVs connected to each phase of the system is random as the utilities do not have a regulation for balancing the number of rooftop PVs among the phases when approving the connection of a rooftop PV to the system. All PVs available in Australian market are equipped with an islanding protection function (e.g. under/over-voltage protection function) based on Australian Standard on grid connection of energy systems via inverters [21] and are required to disconnect after an SCF in the LVF. The output current of the PV systems are equipped with a current limiting technology and protection fuses which limit their output current to 1.5 times of their nominal current [22].

Now, let us assume that a single-phase PV system is connected to one of the phases of the LVF (Fig. 2a). It is intended to investigate the effect of this PV on the protection aspects of the LVF, including the SCF level (I_{Fault}), current supplied from the distribution transformer towards the SCF (I_{DT}), and the voltages of different nodes along the LVF (V). An SCF can occur in the LVF either at PV upstream (Fig. 2b) or downstream (Fig. 2c). In both cases, the fault current is composed of two components: the output current of the PV system and the current supplied by the distribution transformer. Thus, the SCF level increases in the systems of Fig. 2b and 2c with respect to the network of Fig. 2a. A larger increase is observed when the PV system has a higher rating.

For an SCF at PV upstream (Fig. 2b), as the PV is located closer to the end nodes of the LVF, the node in which the PV is installed experiences a greater voltage. This is due to the fact that the output current of the PV passes through a larger portion of the LVF; and thus, a greater voltage appears for every node between the SCF and the PV location. The voltage reduces from the node in which the PV is located towards the SCF point. For a bolted SCF (in which the SCF impedance is zero), the PV presence does not have any impact on the voltages of the nodes between the distribution transformer and the SCF location. In addition, it does not affect the current supplied by the distribution transformer. It is to be reminded that for a realistic SCF (with a small impedance but not zero), the current supplied by the PV system will cause an increase in the voltage of the node in which the SCF has occurred. This slightly increased voltage will reduce the current supplied by the distribution transformer marginally. A stronger impact is detected when the PV has a larger rating.

For an SCF at PV downstream (Fig. 2c), the voltage at the node in which the PV is located is increased compared to the system of Fig. 2a; and thus, the current supplied by the distribution transformer reduces. As the PV is located closer to the

beginning nodes of the LVF, the impact becomes stronger. Thus, the SCF level reduces slightly; however, it is still larger than the SCF level of Fig. 2a. A larger impact is observed for a PV with a higher rating.

3. System Modeling and Analysis

Fig. 1b depicts the equivalent electric circuit representation of Fig. 1a. The network of Fig. 1b resembles a traditional three-phase power system if the PV systems are ignored. However, the network of Fig. 1b is assumed to have single-phase PV systems in which the number of the PVs per each phase and each node of the system may be unequal. Furthermore, each PV may have a different rating and output power compared to the other PVs of the network. Hence, the network of Fig. 1b is considered as an unbalanced network and has to be analyzed using Fortescue's sequence component method [23], even if the impedances of each phase of the system are identical. In the rest of this section, the network of Fig. 1b is analyzed by sequence components. It is to be highlighted that the main dissimilarity between the considered unbalanced system with the traditional load/feeder-initiated unbalanced systems is the appearance of the negative and zero sequence components of voltage, in addition to its positive sequence, as discussed below:

Assuming an equivalent distance between two adjacent poles (nodes) in the LVF, the LVF impedance matrix can be represented for phase-*A*, *B* and *C* by

$$[\mathbf{Z}_f^{LV}]_{ABC} = z_f.\mathbf{I}_{(3)} \tag{1}$$

where z_f is equal to the per-phase impedance between two adjacent nodes and $\mathbf{I}_{(3)}$ is the identity matrix of order 3. Similarly, the MVF impedance and distribution transformer impedance are represented as

$$[\mathbf{Z}_f^{MV}]_{ABC} = z'_f.\mathbf{I}_{(3)} \tag{2}$$

$$[\mathbf{Z}^{trans}]_{ABC} = z_{trans}.\mathbf{I}_{(3)} \tag{3}$$

where z'_f is equal to the per-phase impedance of the MVF between two adjacent nodes and z_{trans} is the equivalent per-phase impedance of the distribution transformer.

From (1), the LVF impedance in sequence components can be expressed as

$$[\mathbf{Z}_f^{LV}]_{012} = [\mathbf{A}]^{-1}[\mathbf{Z}_f^{LV}]_{ABC}[\mathbf{A}] \tag{4}$$

where $[\mathbf{A}] = \begin{bmatrix} 1 & 1 & 1 \\ 1 & a^2 & a \\ 1 & a & a^2 \end{bmatrix}$ and $a = 1\angle 120°$. In a similar way, the sequence components for the impedance of the MVF and the transformer can be calculated.

Although in dynamic studies, a detailed modeling of all network equipment including PVs is essential, in static analyses,

such as the SCF studies of this research, the network equipment can be modeled with simpler representations of their steady-state performance. From this perspective, the PV systems can be considered as current sources but with proper assumptions such as the maximum output current, or disconnection with respect to voltage variation at their point of coupling during SCFs [16]. Similarly, although the SCF impedance has dynamic characteristics during the SCF [24], these dynamics are ignored in this research. Thus, in the rest of this research, I^{PV} represents the steady-state output current of a PV while Z_{Fault} shows the steady-state value of the SCF impedance. Thereby, the matrix of the output current of PVs connected to phase-*A*, *B* and *C* at node-*i* ($1 \le i \le N$) can be expressed as

$$[\mathbf{I}_i^{PV}]_{ABC} = [I_A^{PV} \quad I_B^{PV} \quad I_C^{PV}]_i^T \tag{5}$$

where *T* is the transpose operator. From (5), the output current of the PVs in each node, in sequence components, is

$$[\mathbf{I}_i^{PV}]_{012} = [\mathbf{A}]^{-1}[\mathbf{I}_i^{PV}]_{ABC} \tag{6}$$

From (4) and (6), for an asymmetrical SCF at node-*k* of the network of Fig. 1b, the equivalent sequence networks are modeled as Fig. 3a. The network is later simplified using the Thevenin-Norton equivalent circuit from the SCF point of view. This simplification is carried out separately for the PVs located at SCF downstream and upstream.

For the PVs at SCF downstream, their output currents are aggregated based on Norton equivalent circuit, as illustrated in Fig. 3b, and expressed as

$$I_{no}^1 = \sum_{i=k}^{n} {I_i^{PV}}^1 \quad , \quad I_{no}^2 = \sum_{i=k}^{n} {I_i^{PV}}^2 \quad , \quad I_{no}^0 = \sum_{i=k}^{n} {I_i^{PV}}^0 \tag{7}$$

where the subscript *no* denotes Norton equivalent.

Thevenin equivalent of the system at SCF upstream, including the PVs, can be depicted as Fig. 3b and expressed as

$$\begin{cases} {V'_{th}}^1 = {V_{Source_{th}}}^1 + \sum_{i=1}^{k-1} {I_i^{PV}}^1 \left({Z_f^{MV}}^1 + {Z^{trans}}^1 + i.{Z_f^{LV}}^1 \right) & {Z_{th}}^1 = {Z_f^{MV}}^1 + {Z^{trans}}^1 + k{Z_f^{LV}}^1 \\ {V'_{th}}^2 = \sum_{i=1}^{k-1} {I_i^{PV}}^2 \left({Z_f^{MV}}^2 + {Z^{trans}}^2 + i.{Z_f^{LV}}^2 \right) & {Z_{th}}^2 = {Z_{th}}^1 \\ {V'_{th}}^0 = \sum_{i=1}^{k-1} {I_i^{PV}}^0 \left({Z^{trans}}^0 + i.{Z_f^{LV}}^0 \right) & {Z_{th}}^0 = {Z^{trans}}^0 + k{Z_f^{LV}}^0 \end{cases} \tag{8}$$

where subscript *th* denotes Thevenin equivalent.

The Thevenin equivalent of the SCF upstream of (8) and the Norton equivalent of the SCF downstream of (7) can be further simplified as Fig. 3c where

$$V_{th}^1 = {V'_{th}}^1 + I_{no}^1 Z_{th}^1 \quad , \quad V_{th}^2 = {V'_{th}}^2 + I_{no}^2 Z_{th}^2 \quad , \quad V_{th}^0 = {V'_{th}}^0 + I_{no}^0 Z_{th}^0 \tag{9}$$

which can be represented as

$$[\mathbf{V}_{th}]_{012} = [\mathbf{V}'_{th}]_{012} + [\mathbf{I}_{no}]_{012} \, [\mathbf{Z}_{th}]_{012} \tag{10}$$

Equation (10) demonstrates that, in addition to the expected negative and zero sequence impedance and positive sequence of voltage, a negative and zero sequence of voltage also appear due to the presence of single-phase PVs that are distributed unequally among the three phases of the network [18].

3.1. SCFs in the Network

The considered SCFs in this paper are LG-F, LL-F and LLG-F (Fig. 4), since they are reported as the most frequent types of SCFs in LVFs [19]. It is to be noted that three-phase-to-ground and open-conductor faults are beyond the scope of this research.

For an LG-F (Fig. 4i-iii), the SCF level is calculated from the current sequence components. For the faulted phase, the SCF level is calculated as

$$[\mathbf{I}^{Fault}]_{ABC} = 3I\,[\lambda_A \quad \lambda_B a^2 \quad \lambda_C a]^T \tag{11}$$

where $I = \dfrac{V_{th}{}^1 + V_{th}{}^2 + V_{th}{}^0}{Z_{th}{}^1 + Z_{th}{}^2 + Z_{th}{}^0 + 3Z_{Fault}}$ while $\lambda_j = 1$ if the LG-F is in phase j ($j = A$, B or C); otherwise it is zero.

After SCF level calculation, the voltage at the SCF location is calculated using Kirchhoff's voltage law (KVL) in sequence components as

$$[\mathbf{V}_{Fault}]_{012} = [\mathbf{V}_{th}]_{012} - [\mathbf{I}]_{012}\,[\mathbf{Z}_{th}]_{012} \tag{12}$$

and is then transferred to ABC frame by

$$[\mathbf{V}_{Fault}]_{ABC} = [\mathbf{A}]_{012}\,[\mathbf{V}_{Fault}]_{012} \tag{13}$$

Finally, the voltage of each node along the LVF of Fig. 2a is calculated.

Likewise, for an LL-F (Fig. 4b), the SCF level is calculated from

$$[\mathbf{I}^{Fault}]_{ABC} = [\mathbf{A}]_{012}[\mathbf{I}_{Fault}]_{012} \tag{14}$$

where $I^1 = \dfrac{V_{th}{}^1 - V_{th}{}^2}{Z_{th}{}^1 + Z_{th}{}^2 + Z_{Fault}}$ while $I^2 = -I^1$ and $I^0 = 0$ if the SCF is between phase-B and C (Fig. 4iv), $I^2 = -I^1\angle + 60$ and $I^0 = 0$ if the SCF is between phase-A and B (Fig. 4v), and $I^2 = -I^1\angle - 60$ and $I^0 = 0$ if the SCF is between phase-A and C (Fig. 4vi).

From the current sequence components, the SCF level and voltage profile along the LVF are then calculated.

Similarly, for an LLG-F, if the SCF is between phase-B and C (Fig. 4vii), the current sequence components are

$$I^1 = \frac{(1+a)\,V_{th}{}^1 + V_{th}{}^2 - Z_{th}{}^2 I^2}{(1+a)\,Z_{th}{}^1} \quad , \quad I^2 = \frac{\beta_1 - \beta_3\beta_4}{\beta_2 - \beta_3\beta_5} \quad , \quad I^0 = -aI^1 - a^2 I^2 \tag{15}$$

where

$$\begin{cases} \beta_1 = V_{th}{}^0 + a^2 V_{th}{}^1 + a V_{th}{}^2 \\ \beta_2 = (1 + a - 2a^2)\, Z_{Fault} + a Z_{th}{}^2 - a^2 Z_{th}{}^0 \\ \beta_3 = (1 + a^2 - 2a)\, Z_{Fault} + a^2 Z_{th}{}^1 - a Z_{th}{}^0 \end{cases} \qquad \beta_4 = \frac{(1+a)\, V_{th}{}^1 + V_{th}{}^2}{(1+a)\, Z_{th}{}^1} \qquad \beta_5 = \frac{Z_{th}{}^2}{(1+a)\, Z_{th}{}^1}$$

while for an LLG-F between phase-*A* and *C* (Fig. 4viii), the current sequence components are

$$I^1 = \frac{V_{th}{}^1 + (1+a) V_{th}{}^2 - Z_{th}{}^2 (1+a) I^2}{Z_{th}{}^1} \quad , \quad I^2 = \frac{\gamma_1 - \gamma_3 \gamma_4}{\gamma_2 - \gamma_3 \gamma_5} \quad , \quad I^0 = -a^2 I^1 - a I^2 \tag{16}$$

where

$$\begin{cases} \gamma_1 = V_{th}{}^0 + a V_{th}{}^1 + a^2 V_{th}{}^2 \\ \gamma_2 = (1 + a^2 - 2a)\, Z_{Fault} + a^2 Z_{th}{}^2 - a\, Z_{th}{}^0 \\ \gamma_3 = (1 + a - 2a^2)\, Z_{Fault} + a\, Z_{th}{}^1 - a^2 Z_{th}{}^0 \end{cases} \qquad \gamma_4 = \frac{V_{th}{}^1 + (1+a)\, V_{th}{}^2}{Z_{th}{}^1} \qquad \gamma_5 = \frac{Z_{th}{}^2 (1+a)}{Z_{th}{}^1} .$$

From the current sequence components, the SCF level and voltage profile along the LVF are then calculated.

3.2. Sensitivity Analysis

The impact of one single-phase rooftop PV on the SCF level of the LVF, as well as the voltage profile along the LVF, is investigated by the sensitivity analysis. PV output power and location in addition to the SCF location are considered as the variables of the sensitivity analysis. In this study, a discrete sensitivity analysis is carried out as the PV output power is assumed to be varied from 0.7 to 3.5 kW in steps of 0.7 kW. The SCF and PV locations are also varied from node-1 to node-*N* =10. The outputs of this analysis are the SCF level, the current sensed at the transformer secondary, and the voltage at each node along the LVF. It is to be noted that only bolted fault conditions are focused within the sensitivity study analysis. The results of this analysis are presented and discussed in Section 4.

A few of the sensitivity analysis results, carried out in MATLAB, were compared with the results of the system modelled in PSCAD/EMTDC. This comparison revealed a maximum of 0.02% error, which validates the accuracy of the system modelling in MATLAB.

3.3. Stochastic Analysis

A deterministic analysis is not comprehensive due to the randomness in PV rating and installation point as well as the SCF location and impedance [25]. Therefore, a MCA is carried out in this paper to investigate and predict the SCF level and the voltage profile along the LVF [26]. The considered uncertainties in the MCA are:

- the PPL in the network,

- the installation point of PVs in each phase and along the LVF,
- the ratings of PVs,
- the SCF location, and
- the SCF impedance,

while the outputs of the MCA analysis are:

- the current sensed at the transformer secondary, and
- the voltage at each node along the LVF.

Fig. 5 illustrates the flowchart of the developed stochastic analysis. As seen from this figure, the SCF-type and PPLs or PV ratings are selected at the beginning and separate MCAs are carried out for each selected combination. PV installation point is assumed to have a uniformly distributed probability over the LVF length (i.e., 400 m in this study which is the typical LVF length in Perth, Australia). They have discrete values of 40 meters (assuming that a 400 m long LVF is distributed over 10 poles with a distance of 40 m from each other). PV ratings are assumed to have discrete values with a normal PDF with an average of 2.5 kW and a variance of 0.8 kW, based on the ratings of the PVs installed in Perth, Australia [17]. The SCF location is assumed to have a PDF similar to that of the PV installation point. Uniform distribution over 0-0.3 Ω is considered for the impedance of the LG-Fs while the impedance of the LL-Fs and LLG-Fs are assumed to have a historical data-supported PDF of Fig. 6a-b [19].

To reduce and eliminate the non-desired combinations of the inputs for the stochastic analysis, a *Time* parameter, depicted in Fig. 7, is considered which represents the time of the study over the 24-hr period and is normalized in the range of 0 to 1. In this study, the sunlight availability is assumed between 6 am and 19 pm while the PVs generate their maximum output at 12 pm with the coefficient factor of 1, considering the sun radiation in Perth, Australia [27]. *Time* is utilized to select correlated random values for the instantaneous output current available from PVs while the other inputs of the MCA are considered independent of *Time* [28-29]. Alternatively, the methods proposed in [30-31] can be utilized to determine the PV output power based on solar irradiance. In this study, all inputs of the MCA are produced using different random generation codes of MATLAB, considering the above-mentioned PDFs.

The termination criterion of the MCA is chosen based on achieving an acceptable convergence for the average and variance of the desired outputs (SCF level, and node voltages along the LVF). For this, the MCA simulation is deemed converged when a confidence degree of 95% is achieved. However, a minimum of 10,000 trials is utilized to avoid premature convergence. Once the MCA is converged, the PDF is defined for all desired outputs. The PDF is described in terms of the distribution function, the expected average voltage (EAV) and standard deviation (STD) of each output from all iterations.

It is to be noted that if large networks such as the IEEE 342-node North American LVF and 906-node European LVF standard test cases in [32] are considered, the computation of the equivalent sequence components of the voltage and impedance in (7)-(16) may become complicated; however, the duration of MCA will not be prolonged significantly as its execution time depends on the number of its inputs and its considered termination criteria.

3.4. Maximum Allowed PPL

Based on the findings from the stochastic analysis, the study aims to investigate the maximum allowed PPL in a residential LVF from the SCF perspective (note that other considerations such as the maximum voltage rise and maximum harmonic distortion in the LVF should also be considered when selecting a general limit). To this end, different criteria may be defined. This study has determined the maximum allowed PPL as the function of two criteria, namely switch-fuse operation probability (SOP), and PV disconnection probability (PDP). The SOP illustrates the probability of operation of the switch-fuse (at the secondary of the distribution transformer) in the case of an SCF, while the PDP depicts the probability of disconnection of PVs of the LVF after an SCF because of voltage deviation at the connection point of the PV, according to IEEE Standard 929-2000 [33]. From the MCA-derived PDF for node voltages (considering its EAV and STD), the probability of observing a voltage higher than 1.1 or below 0.88 per-unit (pu), i.e., the thresholds for the disconnection of a PV according to [33], is calculated and referred to as the PDP. Similarly, using the derived PDF for the current sensed at the transformer secondary (considering its EAV and STD), the probability of observing a current higher than 1.25 pu (i.e., the threshold for the operation of the switch-fuse) is calculated, and referred to as the SOP. These two indices are expressed for different PPLs at various SCF types. From the SCF perspective, the maximum allowed PPL is then determined as the corresponding PPL for the minimum probability of the successful operation of the switch-fuse or the disconnection of PVs, after an SCF in the LVF.

4. Sensitivity Analysis Results

The sensitivity analysis evaluates the effect of one single-phase PV on the SCF level, the current sensed at the transformer secondary and the voltage profile along the LVF, during an LG-F on phase-*A* as well as an LL-F and LLG-F on phase-*A* and *B*, all assuming $Z_{Fault} = 0$. The sensitivity analysis is carried out in MATLAB while a few of the cases studies are remodelled in PSCAD/EMTDC, and the results are compared to validate the accuracy of MATLAB modelling.

4.1. Voltage Profile

A parameter that plays a major role in disconnection of PVs following SCFs in the LVF is the voltage at the PV connection point. In this section, the deviation of the voltage along LVF in the presence of a PV is investigated during SCFs.

Let us consider the network of Fig. 1b without any PVs which is referred to as the 'No-PV' case in the rest of the paper. Now let us consider a single-phase PV with a rating of 2 kW (i.e., approximately 8.3 A at 240 V with a unity power factor).

The output current of the PV is limited to 150% of its nominal rating (12.5 A) during the SCF. The network in the presence of this PV is referred to as the 'PV-available' case in the rest of the paper. Let us assume an LG-F on phase-*A* at the beginning of the feeder (BOF), i.e., node-1, while the PV is located at different nodes along the LVF (node-1 to 10). The voltage of the nodes along the LVF in the PV-available case is more than the No-PV case. Let us define the voltage difference (VD) as the voltage of the PV-available case minus the voltage of the No-PV case during the SCF. The VD is shown in Fig. 8a, and illustrates that the end nodes of the LVF experience a greater VD compared to the beginning nodes. The reason for this increase is that as the PV is located closer to the end of the feeder (EOF) i.e., node-10, its output current passes through a larger portion of the LVF and a greater voltage appears for every node between the SCF and the PV location. Also, it can be seen that VD increases from feeder beginning towards PV location; however, it is not affected for the nodes at PV downstream. Also, the greatest VD is seen when the PV is located at feeder far end nodes.

Now, let us assume the SCF is at the EOF. In this case, the VD is much smaller compared to the case in which the SCF is at node-1 (Fig. 8b). The VD increases from the feeder beginning towards the PV location and then decreases towards the SCF location. This is because only the current supplied from the distribution transformer flows between the distribution transformer and the PV location while the currents of both of the PV and the distribution transformer flow between the PV and SCF locations. Thus, a larger voltage appears on the downstream nodes of PV location. The greatest VD is detected when the PV is in the middle of the feeder (MOF), i.e., node-5.

Let us now assume the SCF is at the MOF. When the PV is at SCF upstream, the VD has a similar trend to the one shown in Fig. 8a while a similar pattern to the one in Fig. 6b is witnessed when the PV is at SCF downstream (Fig. 8c). This observation can also be justified based on the abovementioned facts.

To investigate the effect of PV rating, let us assume an LG-F at node-8 where a PV, located at node-4, is assumed to have a rating of 0.7 to 3.5 kW. In this case, with the increase of the PV output power, a greater VD is observed (Fig. 8d). This is because a PV with a higher rating has a larger output current, and consequently a greater voltage appears.

Another analysis is carried out for LL-Fs. Let us consider an SCF at the BOF. In this case, the VD trend is similar to the results of LG-F but almost half of that (Fig. 9a). Assuming the SCF location at the EOF, the VD variation is greater at PV upstream side and lower at PV downstream side (Fig. 9b). Also, the VD is greater as the PV is closer to the EOF.

Now let us assume an LL-F at the MOF. In this case, two trends are seen for the VD. In the cases that the PV is at SCF downstream, the VD increases towards the EOF. For the cases in which the PV is at SCF upstream, the VD is high for the nodes at PV upstream and low for the nodes at PV downstream (Fig. 9c).

Let us now assume a PV with a rating of 0.7-3.5 kW. The PV is installed at node-4, and the SCF occurs at node-8. In this

case, the VD on the nodes at the SCF downstream is not affected by the PV rating. However, it is increased on the nodes at the SCF upstream for large PV ratings (Fig. 9d).

Sensitivity analysis results show that the VD trend for an LLG-F is similar to LG-Fs and is not repeated.

4.2. Transformer Current and SCF Level

Another important factor for the protection of LVFs in the case of SCFs is the current sensed by the switch-fuses at the secondary side of the distribution transformers. Any deviation in the current sensed at the secondary side of the distribution transformers will cause a deviation in the tripping time of the switch-fuse. This deviation is investigated in this section in the presence of a PV in the system.

Let us again consider a 2 kW PV with 150% current limiting during the SCF. The SCF and PV location are varied from node-1 to 10. Let us define the fault current difference (FCD) as the SCF level in PV-available case minus the SCF level at No-PV case. Similarly, let us define the transformer current difference (TCD) as the current sensed at the transformer secondary in PV-available case minus the No-PV case.

For the SCFs at PV downstream, as the SCF moves towards the EOF, the FCD decreases (Fig. 10a). This can be explained by the variation of the voltages of the nodes as a result of SCF location which consequently affects the current supplied by the distribution transformer. For the SCFs at PV upstream, as the SCF moves from the BOF towards the PV location, the FCD increases (Fig. 10a). The highest FCD is detected when the SCF is at the PV connection node.

When the PV is at SCF upstream, the current sensed at the transformer secondary in the PV-available case is lower than the No-PV case (Fig 10b). Hence the TCD is negative. This is because the voltage at the PV connection point compared to the No-PV case which leads to a smaller current drawn from the source. When the PV is at SCF downstream, there is no difference between transformer secondary current in No-PV and PV-available cases; hence, the TCD is zero (Fig. 10b). This is due to the fact that the PV does not affect the voltages at SCF upstream. As the PV is closer to feeder beginning nodes, the transformer secondary current is much less than that of the No-PV case.

Now, let us assume an LG-F at node-8 where a PV, located at node-4, has a rating of 0.7 to 3.5 kW. As the PV rating increases, the FCD becomes greater (Fig. 9c) while a TCD reduces more (Fig. 10d).

For an LL-F at feeder beginning nodes regardless of the PV location, the SCF level in the PV-available case is larger than the No-PV case; hence, the FCD is positive (Fig. 11a). The FCD is negative when the SCF is at feeder end nodes. For the SCF at the feeder end nodes, as the PV is relocated from the BOF towards the SCF location, the FCD increases. However, it is constant if the PV is at SCF downstream. When the SCF is at the feeder beginning nodes, the FCD decreases as the PV is relocated from the BOF towards the SCF location. However, it is zero if the PV is at SCF downstream.

For an LL-F, the transformer secondary current in the PV-available case is less than the No-PV case; thus, the TCD is negative (Fig. 11b). This is due to the fact that the voltage at the node in which the PV has located increases because of the PV; thus, the current supplied by the distribution transformer reduces. For the LL-Fs, as the PV is relocated from the BOF towards the SCF location, the TCD decreases. However, it is constant if the PV is at SCF downstream (Fig. 11b).

Now, let us assume an LL-F at node-8 where a PV, located at node-4, has a rating of 0.7 to 3.5 kW. In such a case, for lower PV ratings (e.g. lower than 2.8 kW), the FCD is negative while it is positive for large PV ratings (e.g. 3.5 kW). As the PV rating increases, the FCD decreases (Fig. 11c). For lower PV ratings (e.g. lower than 1.4 kW), the TCD is positive (Fig. 11d) while it is negative for large PV ratings (e.g. larger than 2.1 kW).

Now, let us assume an LL-F at node-4 while the PV is at node-8. In such a case, the FCD is always positive and increases for large PV output powers (Fig. 11e). Although the TCD rises with respect to an increase in the PV output power, it is negative (Fig. 11f). This can be explained by the fact that when the PV is located at SCF downstream, the voltage of the node in which the SCF is applied is higher than the No-PV case. A greater difference is observed for larger PV ratings, and consequently, the current supplied by the distribution transformer reduces. In addition, the voltage of PV connection point increases and the current supplied by the transformer reduces.

For an LLG-F, the FCD increases as the PV is closer to the SCF location; however, it is almost constant if the PV is at the downstream of SCF (Fig. 12a). During an LLG-F, if the PV is at SCF downstream, the TCD is zero. However, if the PV is at SCF upstream, the TCD reduces as the PV is relocated from the BOF towards the SCF location. Assuming the PV is located at one node, the TCD increases as the SCF location varies from the PV towards the EOF (Fig. 12b).

Now, let us assume an LLG-F at node-8 where a PV, located at node-4, has a rating of 0.7 to 3.5 kW. In such a case, the FCD is negative and increases for large PV ratings (Fig. 12c). However, it is almost constant for PV ratings of higher than 2.1 kW. On the other hand, the TCD is negative and experiences an increase in large PV ratings (Fig. 12d).

Let us now assume an LLG-F at node-4 when the PV is at node-8. In such a case, the FCD is negative and almost same if the PV rating is lower than 2.8 kW while it is positive for PV ratings of higher than 3.5 kW (Fig. 12e). The TCD in this condition is zero for all PV ratings (Fig. 12f).

5. Stochastic Analysis Results

The stochastic analysis evaluates the effect of multiple PVs at different locations and phases, various PPLs and instantaneous output power of PVs during all types of SCFs. In this study, transformer secondary current and voltages at each node are the desired outputs, for which their EAV and STD values are presented instead of their PDF figures.

5.1. Voltage Profile

First, the MCA is carried out for an LG-F, LL-F and LLG-F, assuming a PPL of 50%. Depending on the *Time* parameter, different instantaneous output powers are selected for the PVs in the MCA iterations. The results of this analysis at the BOF, MOF, and EOF of the faulted phase are shown in Table 1. As seen from this table, the EAV of each node has a slight increase for large PV ratings. Note that there is no significant variation in the STD due to the change in PV ratings. For LL-Fs and LLG-Fs, the data of one of the faulted phases has been captured. The results for LL-F show a decrease in the EAVs of each node for large PV ratings. The STD of the node voltages also goes down as the PV rating increases. Also, this table reveals that the expected average and STD of the voltages at the BOF increase for large PV ratings; however, they decrease at the MOF and EOF.

Another MCA is carried out assuming that all PVs have an output power of 2 kW with a 150% current limiting while different PPLs are considered. The results of this analysis are also given in Table 1 which shows that in the case of LG-Fs, the EAV of each node increases for large PPLs, but it is not considerable. Also, for large PPLs, the STD for node voltages slightly increases. It can be seen for LL-F that with an increase in PV rating and PPL, the EAV of the nodes and their STD also increase. In the case of LLG-Fs, the EAV at BOF increases for large PPLs; however, it decreases at the MOF and EOF. The STD of voltages in all nodes increases for large PPLs.

Table 2 lists the EAV of each node of the LVF for different PPLs under various SCF types. Through this chart, it can be seen that the phase voltages on the faulted phase are below the threshold of 0.88 pu for both LG-Fs and LLG-Fs, regardless of the PPL. However, the EAV of the nodes at the BOF is above the threshold. Using the corresponding PDFs, the PDP is also calculated for each node of the LVF, and listed in Table 2. From this analysis, it can be seen that the PVs in the faulted phase will disconnect according to [33] in the case of LG-Fs and LLG-Fs with a probability of over 89%. However, this probability is between 52-63% in the case of LL-F. In this type of SCF, the impact of the PPL is more tangible, and it increases to large PPLs.

5.2. Transformer Current

The above MCAs are repeated to investigate the expected PDF of the current sensed at the transformer secondary during the SCF. The results of these analyses are given in Table 3 which shows that PV ratings and PPLs do not modify the expected average current at transformer secondary during an LG-F. In addition, the increase in the STD with respect to the increase of PV rating and PPL is not significant. For an LL-F, it can be seen that the average and STD of transformer current increases for large PV ratings or PPLs while they decrease for an LLG-F.

Table 3 also illustrates the calculated SOP to each SCF-type. It can be seen that the SOP is same for all PPLs in every SCF-type, varying from 99 and 97% in the case of LLG-Fs and LG-Fs respectively to 89% in the case of LL-Fs. Based on this table, it can be concluded that the switch-fuse at the transformer secondary will detect the SCF in the LVF successfully with a

probability of over 89%.

6. Discussion

The sensitivity analysis shows that the voltages of nodes, the transformer secondary current, and the SCF level depend on the SCF and PV location along the LVF. It is seen that the presence of a PV at SCF upstream has different impacts on these three parameters, compared to the case in which the PV is at SCF downstream. It is also observed that these effects are not similar for LG-Fs, LL-Fs, and LLG-Fs.

The results of the sensitivity analysis demonstrate that the SCF level is always higher when a PV is present in the LVF for an LG-F but it may be lower or greater in LL-Fs and LLG-Fs, depending on the SCF and PV location. Interestingly, it can be understood that the PV rating has an entirely different impact on the transformer secondary current and SCF level even in the same SCF-type and location as well as the same PV location.

During LG-Fs and LLG-Fs, the current observed at the secondary of the distribution transformer is reduced when a PV is present in the network, and a larger difference is seen when the SCF is closer to the EOF. However, for LL-Fs, a greater change is seen when the SCF is at the MOF. As the current sensed at the transformer secondary is reduced, the operation time of the switch-fuse is expected to be delayed slightly.

The ratio of STD to the EAV or expected average current represents the data diversity in each of the conducted MCA studies. Table 1 shows that this ratio is below 18% for LL-Fs and LLG-Fs while it is in the range of 23-52% for LG-Fs. It can also be seen that this ratio is in the range of 7-24% when the SCF is at the BOF while it is in the range of 12-40% and 15-52% for the SCFs at the MOF and EOF, respectively. Thus, it can be concluded that the SCF impedance and location (with the assumed PDFs) are the dominant inputs than the PV rating and PPL. Also, it can be concluded that as the SCF is located closer to the far end nodes of the LVF, the data diversity increases as other inputs also become more influential. Likewise, from Table 3, this ratio is determined to be in the range of 32-62% which again emphasizes that SCF location and impedance are the dominant inputs.

Table 4 summarizes the results of the MCA for three types of SCFs and shows the impact of PV rating and PPL increase on the EAV of the nodes along the LVF, and the average of the transformer secondary current. The stochastic analysis results demonstrate that the EAV of the PDF of the transformer secondary current increases during LL-F and decreases in LLG-F, for large PV ratings or PPLs. However, it does not demonstrate a particular trend for LG-Fs.

An increase in PPL leads to an increase of the EAV of the nodes in LG-Fs while it causes a decrease in these parameters during LL-Fs. Similarly, the increase in PV rating results in an increase of this parameter in case of the LG-Fs but a decrease for LL-Fs. On the other hand, in the case of LLG-Fs, for large PV ratings or PPLs, the EAV of nodes increase at BOF and decrease

at the MOF or EOF.

It is to be noted that the stochastic analysis considers different parameters of SCF location and impedance, PV installation point and rating, and PPL as the input and its outcome illustrates the combined impact of all inputs. As seen from Table 1-3, the outcomes of the MCA are not too different when varying the PPL from 0 to 100%. This implies that other inputs (mainly the SCF impedance and location) have a stronger impact on the outcome as they are directly related, while the outcomes are not directly influenced by the PPL. On the other hand, the output currents of the PVs are limited to 150% of their nominal current during SCFs, and the variation of the PPL does not change it significantly when compared with the SCF level of the network. Thereby, it is seen that the PPL is not a strong measure when evaluating the performance of an LVF under SCFs.

Table 3 shows that the SOP is above 89% for LG-Fs, LL-Fs, and LLG-Fs irrespective of the PPL. On the other hand, Table 2 indicates that the PDP is above the same level for LG-Fs and LLG-Fs while it is between 52-63% for LL-Fs. Thereby, considering only the SOP criterion, even at a PPL of 100%, the switch-fuse at the transformer secondary will detect the SCF in the LVF successfully with a probability of over 89%. However, considering the PDP criterion for all considered SCF types, a PPL of below 80% will result in the disconnection of the PVs on the faulted phase with a probability of approximately 52-57% while this number rises to 60-63% for a PPL of above 80%.

7. Conclusion

This research has evaluated the contribution of residential single-phase rooftop PVs on the SCFs in the supplying LVFs. The typical Australian LVFs have been focused in this study. The effect of PVs on the voltage profile along the LVF and the current sensed at the secondary of the distribution transformer is studied during LG-Fs, LL-Fs, and LLG-Fs. A sensitivity analysis is carried out in MATLAB where its accuracy is verified in comparison with PSCAD/EMTDC results. Later, to consider the uncertainties in PV rating, location, and PPL as well as the SCF location and impedance, a stochastic analysis is carried out.

Three parameters of SCF level, transformer current, and voltages of the nodes along the LVF are investigated during SCFs on typical Australian LVFs. The FCD, TCD, and VD variables respectively show the dissimilarity between these three parameters in the network with and without a PV. Through the sensitivity analyses, it is concluded that the SCF level increases by 10% when a PV is present in the LVF while the transformer secondary current may decrease by 7%. The results of the stochastic analysis show that the expected average current at transformer secondary and EAV of the nodes along the LVF are not influenced strongly by the PV ratings and PPLs, and it is seen that the SCF location and impedance are the dominant factors to be considered.

Based on the outcomes of the MCA, two criteria were defined. They were used to evaluate the impact of the PV rating and

PPL on the probability of the successful detection of SCF by protective devices. The considered protective devices are the switch-fuse at the transformer secondary, and the disconnectors at the PV output. The defined criteria show that, with a probability of over 89%, the switch-fuse will detect the SCFs on typical Australian LVFs. It also shows that with a minimum probability of 52-57%, the disconnectors will isolate the PVs when the PPL is below 80%. However, PPL of higher than 80% increases the PV disconnection probability to 60-63%.

As highlighted earlier, this study had focused on typical Australian LVFs in which an LVF is a three-phase, four-wire, MEN system, supplied by three-phase distribution transformers. Even though a distribution transformer may have multiple feeders at its output, each feeder is three-phase throughout its length and does not have laterals. However, these may not be valid for the LVFs in all countries. As a future research topic, other networks such as the IEEE 342-node North American LVF and the 906-node European LVF standard test cases can be chosen as the network under study, and the analysis can be repeated to compare its outcomes with the findings for this research. Also, the outcomes of the study can be expanded in another research to derive a general criterion to determine the maximum PPL in LVFs when also considering the voltage rise and total harmonic distortion impacts of the PVs.

Appendix

The technical data of the network under consideration in Fig. 1b are listed in Table A1.

References

[1] Australian Energy statistics - Energy Update, 2011.
http://data.daff.gov.au/data/warehouse/pe_abares99010610/EnergyUpdate_2011_REPORT.pdf

[2] L. Romanach, Z. Contreras, and P. Ashworth, "Australian householders' interest in the distributed energy market –National survey results", CSIRO report prepared for the Australian Photovoltaic Association, 2013.
http://www.csiro.au/Organisation-Structure/Flagships/Energy-Flagship/Australian-householders-interest-in-the-distributed-energy-market.aspx

[3] M.J.E. Alam, K.M. Muttaqi, and D. Sutanto, "An approach for online assessment of rooftop solar PV impacts on low-voltage distribution networks," *IEEE Trans. Sustainable Energy*, vol.5, Issue.2, pp.663-672, 2014.

[4] G. Mokhtari, G. Nourbakhsh, F. Zare, and A. Ghosh, "Improving the penetration level of PVs using dc link for residential buildings," *Energy and Buildings*, vol.72, pp.80-86, 2014.

[5] F. Shahnia, R. Majumder, A. Ghosh, *et al.*, "Voltage imbalance analysis in residential low voltage distribution networks with rooftop PVs," *Electric Power Systems Research*, vol.81, Issue.9, pp.1805-1814, 2011.

[6] F. Shahnia, A. Ghosh, G. Ledwich, and F. Zare, "Voltage unbalance improvement in low voltage residential feeders with

rooftop PVs using custom power devices," *International Journal of Electrical Power & Energy Systems*, vol.55, pp.362-377, 2014.

[7] G. Mokhtari, G. Nourbakhsh, F. Zare, and A. Ghosh, "Overvoltage prevention in LV smart grid using customer resources coordination," *Energy and Buildings*, Vol.61, pp.387-395, 2013.

[8] B. Noone, "PV integration on Australian distribution networks: Literature review," Australian PV Association, 2013.

[9] V. Calderaro, S. Corsi, V. Galdi, and A. Piccolo, "Optimal setting of the protection systems in distribution networks in presence of distributed generation," 40th Int. Universities Power Engineering Conf., 2005.

[10]A. Alkuhayli, S. Raghavan, and B.H. Chowdhury, "Reliability evaluation of distribution systems containing renewable distributed generations," North American Power Symposium (NAPS), pp.1-6, 2012.

[11]P.K. Ray, *et al.*, "Optimal feature and decision tree based classification of power quality disturbances in distributed generation systems," *IEEE Trans. Sustainable Energy*, vol.5, Issue.1, pp.200-208, 2014.

[12]K. Maki, S. Repo, and P. Jarventausta, "Protection planning development for DG installations," 20th Int. Conf. on Electricity Distribution, 2009.

[13]*Guide to conducting distribution impact studies for distributed resource interconnection*, IEEE Std. 1547.7, 2012.

[14]R.A. Walling, R. Saint, R.C. Dugan, *et al*., "Summary of distributed resources impact on power delivery systems," *IEEE Trans. Power Delivery*, Vol.23, Issue.3, pp.1636-1644, 2008.

[15]B. Subhashish, T. Saha, and M.J. Hossein, "Fault current contribution from photovoltaic systems in residential power networks," 23rd Australian University Power Engineering Conf. (AUPEC), 2013.

[16]M.E. Baran, H. Hooshyar, Z. Shen, *et al.*, "Impact of high penetration residential PV systems on distribution systems," IEEE Power and Energy Society General Meeting, pp.1-5, 2011.

[17]Perth solar city annual report, 2011.
http://www.westernpower.com.au/documents/psc_-_2012_annual_report_-_final_for_distribution_(lo-res_18.pdf

[18]H.H. Yengejeh, F. Shahnia, and S.M. Islam, "Contributions of single-phase rooftop PVs on short circuits faults in residential feeders," 24th Australian University Power Engineering Conf. (AUPEC), pp.1-6, 2014.

[19]V. Garcia, J.C. Cebrian and N. Kagan, "Evaluation of probability functions related to short circuit random variables using power quality meters," IEEE/PES Transmission & Distribution Conf. Latin America, 2010.

[20]Energex/Ergon Energy connection standard on Small Scale Parallel Inverter Energy Systems up to 30 kVA, 2014.
https://www.ergon.com.au/__data/assets/pdf_file/0005/198698/STNW1170ver2-Connection-Standard-for-IES-up-to-30kVA.pdf

[21]Australian Standard on Grid Connection of Energy Systems via Inverters, AS 4777, Draft version, 2013.

[22]Photovoltaic system protection application guide, 2012.

http://www1.cooperbussmann.com/pdf/1b416a65-f5ac-4730-ab77-9e2faa147945.pdf

[23]J.G. Grainger, and W.D. Stevenson Jr. *Power System Analysis*, McGraw-Hill, 1994.

[24]M. Dewadasa, *Protection of Distributed Generation Interfaced Networks*, PhD Thesis, Queensland University, 2010.

[25]F. Shahnia, A. Ghosh, G. Ledwich, and F. Zare, "Predicting voltage unbalance impacts of plug-in electric vehicles penetration in residential low voltage distribution networks," *Electric Power Components and Systems*, vol.41, Issue.16, pp.1594-1616, 2013.

[26]C. Robert and G. Casella, *Monte Carlo Statistical Methods*, Springer, 2004.

[27]Average annual and monthly sunshine duration, Bureau of Metrology,

http://www.bom.gov.au/jsp/ncc/climate_averages/sunshine-hours/index.jsp

[28]H.H. Yengejeh, F. Shahnia, and S. Islam, "Disconnection time and sequence of rooftop PVs under short-circuit faults in low voltage networks," North American Power Symposium (NAPS), pp. 1-6, Charlotte, USA, 2015.

[29]H.H. Yengejeh, F. Shahnia, and S.M. Islam, "Disconnection of single-phase rooftop PVs after short-circuit faults in residential feeders," *Australian Journal of Electrical & Electronics Engineering*, vol.13, no.2, pp.151-165, 2016.

[30]N. Nikmehr, and S. Najafi-Ravadanegh, "Optimal power dispatch of multi-microgrids at future smart distribution grids," *IEEE Trans. Smart Grid*, vol.6, no.4, pp.1648-1657, 2015.

[31]T. Ishii, K. Otani, T. Takashima, and S. Kawai, "Estimation of the maximum power temperature coefficients of PV modules at different time scales," *Solar Energy Materials and Solar Cells*, vol.95, no.1, pp.386-389, 2011.

[32]Distribution Test Feeders, IEEE PES distribution system analysis subcommittee's distribution test feeder working group, 2016. https://ewh.ieee.org/soc/pes/dsacom/testfeeders/

[33]IEEE Recommended Practice for Utility Interface of Photovoltaic (PV) Systems, IEEE Standard 929-2000.

[34]Olex aerial conductors catalog, 2012. http://www.olex.com.au/Australasia/2012/OLC12641_AerialCat.pdf

Table 1. MCA results for the node voltages [pu] of the faulted phase in different PV ratings and PPLs under various SCF types.

Fault	PV [kW]	BOF		MOF		EOF		PPL [%]	BOF		MOF		EOF	
		EAV	STD	EAV	STD	EAV	STD		EAV	STD	EAV	STD	EAV	STD
LG-F	0.7	0.7482	0.1742	0.5578	0.2236	0.4865	0.2513	20	0.7481	0.1733	0.5583	0.2229	0.4882	0.2516
	1.4	0.7492	0.1739	0.5605	0.2239	0.4904	0.2525	40	0.7492	0.1745	0.5615	0.2242	0.4893	0.2518
	2.1	0.7514	0.1736	0.5632	0.2247	0.4932	0.2537	60	0.7502	0.1760	0.5635	0.2253	0.4902	0.2536
	2.8	0.7547	0.1746	0.5675	0.2255	0.4962	0.2543	80	0.7551	0.1756	0.5697	0.2258	0.4977	0.2549
	3.5	0.7568	0.1751	0.5704	0.2247	0.4991	0.2539	100	0.7580	0.1763	0.5715	0.2265	0.5018	0.2552
LL-F	0.7	0.9552	0.0693	0.8639	0.1193	0.8354	0.1400	20	0.9551	0.0702	0.8641	0.1202	0.8360	0.1405
	1.4	0.9475	0.0687	0.8537	0.1191	0.8238	0.1401	40	0.9482	0.0697	0.8551	0.1192	0.8255	0.1399
	2.1	0.9395	0.0677	0.8425	0.1187	0.8115	0.1394	60	0.9425	0.0668	0.8462	0.1183	0.8157	0.1392
	2.8	0.9316	0.0669	0.8319	0.1175	0.7999	0.1383	80	0.9331	0.0658	0.8340	0.1172	0.8020	0.1386
	3.5	0.9262	0.0651	0.8250	0.1165	0.7923	0.1373	100	0.9246	0.0650	0.8230	0.1167	0.7900	0.1378
LLG-F	0.7	0.5354	0.0917	0.4625	0.0583	0.4469	0.0700	20	0.5357	0.0913	0.4626	0.0536	0.4467	0.0687
	1.4	0.5393	0.0930	0.4604	0.0568	0.4413	0.0683	40	0.5395	0.0926	0.4599	0.0539	0.4405	0.0689
	2.1	0.5418	0.0942	0.4577	0.0565	0.4355	0.0679	60	0.5423	0.0938	0.4568	0.0546	0.4347	0.0694
	2.8	0.5461	0.0965	0.4552	0.0561	0.4294	0.0667	80	0.5468	0.0963	0.4554	0.0550	0.4294	0.0695
	3.5	0.5487	0.0973	0.4534	0.0556	0.4251	0.0662	100	0.5489	0.0971	0.4533	0.0552	0.4244	0.0699

Table 2. EAV of all nodes of the LVF and the corresponding PDP in various PPLs and different SCFs.

Fault	PPL [%]	EAV [%] at node-										PDP [%] at node-										PDP [%]
		1	2	3	4	5	6	7	8	9	10	1	2	3	4	5	6	7	8	9	10	
LG-F	20	74.8	68.3	63.1	58.8	55.8	55.4	52.6	50.6	49.2	74.8	77.7	84.9	88.9	91.4	92.6	92.1	93.1	93.7	94.0	94.1	90.3
	40	74.9	68.4	63.3	59.0	56.1	55.5	52.8	50.8	49.4	74.9	77.4	84.5	88.7	91.2	92.3	92.0	92.9	93.5	93.9	94.0	90.1
	60	75.0	68.8	63.7	59.5	56.3	56.0	53.4	51.4	50.0	75.0	77.0	84.1	88.2	90.7	92.1	91.5	92.5	93.1	93.5	93.8	89.7
	80	75.5	68.9	63.8	59.6	56.9	56.0	53.6	51.6	50.2	75.5	76.2	83.8	87.9	90.4	91.6	91.2	92.2	92.9	93.2	93.4	89.3
	100	75.8	69.4	64.4	62.0	57.1	56.8	54.1	52.1	50.7	75.8	75.6	83.3	87.5	90.1	91.4	90.9	92.0	92.6	93.0	93.2	89.0
LL-F	20	95.5	92.4	89.8	88.2	86.4	85.1	84.3	83.8	83.5	83.6	14.3	48.0	49.3	49.9	55.3	59	61.0	62.1	62.7	62.4	52.4
	40	94.8	91.6	89.0	87.3	85.5	84.2	83.3	82.8	82.5	82.5	16.5	48.3	49.6	52.6	58.3	61.8	63.8	64.8	65.4	65.3	54.7
	60	94.2	97.0	88.0	85.9	84.6	83.0	82.2	81.6	81.3	81.5	17.7	48.8	50.0	57.7	61.3	65.4	67.0	68.1	68.6	68.0	57.3
	80	93.3	89.9	87.2	85.0	83.4	82.0	81.1	80.5	80.2	80.2	21.1	49.1	50.4	61.1	65.2	68.4	70.2	71.2	71.6	71.5	60.0
	100	92.4	89.1	86.3	84.1	82.3	81.1	80.2	79.6	79.2	79.0	25.0	49.5	50.8	64.4	68.7	71.0	72.7	73.5	74.1	74.5	62.5
LLG-F	20	53.5	59	48.9	47.3	46.2	45.4	45.0	44.7	44.6	44.6	99.9	100	100	100	100	100	100	100	100	100	99.9
	40	53.9	51.1	48.9	47.2	45.9	45.0	44.5	44.2	44.1	44.0	99.9	100	100	100	100	100	100	100	100	100	99.9
	60	54.2	51.3	48.9	47.1	45.6	44.8	44.1	43.8	43.6	43.4	99.9	100	100	100	100	100	100	100	100	100	99.9
	80	54.6	51.5	49.0	47.0	45.5	44.4	43.7	43.2	43.0	42.9	99.9	100	100	100	100	100	100	100	100	100	99.9
	100	54.8	51.7	49.0	46.9	45.3	44.0	43.2	42.7	42.5	42.4	99.9	100	100	100	100	100	100	100	100	100	99.9

Table 3. MCA results for current at the transformer secondary [pu] of different SCF types and the expected operation probability of the switch fuse [%].

Fault	PV [kW]	Transformer Current average	Transformer Current STD	PPL [%]	Transformer Current average	Transformer Current STD	SOP [%]
LG-F	0.7	6.9221	2.9889	20	6.9381	2.9884	0.97
	1.4	6.9364	2.9944	40	6.9336	2.9904	
	2.1	6.9421	2.9819	60	6.9490	2.9949	
	2.8	6.9227	3.0054	80	6.9040	3.0230	
	3.5	6.9328	3.0312	100	6.9050	3.0412	
LL-F	0.7	4.8637	2.9879	20	4.8413	2.9862	0.89
	1.4	4.8810	2.9948	40	4.8655	3.0103	
	2.1	4.8927	3.0241	60	4.9017	3.0168	
	2.8	4.9465	3.0275	80	4.9224	3.0206	
	3.5	4.9534	3.0289	100	4.9327	3.0293	
LLG-F	0.7	8.7255	2.8067	20	8.7538	2.8227	0.99
	1.4	8.7156	2.8037	40	8.7405	2.8111	
	2.1	8.7041	2.7928	60	8.6751	2.7859	
	2.8	8.6715	2.7885	80	8.6642	2.7756	
	3.5	8.6608	2.7770	100	8.6464	2.7676	

Table 4. Summary of stochastic analyses for different faults in the network.

Fault	MCA Output	Variable	Expected average	STD
LG-F	Transformer Current	PV Rating	~	~
		PPL	~	↑
	Voltage	PV Rating	↑	~
		PPL	↑	↑
LL-F	Transformer Current	PV Rating	↑	↑
		PPL	↑	↑
	Voltage	PV Rating	↓	↓
		PPL	↓	↓
LLG-F	Transformer Current	PV Rating	↓	↓
		PPL	↓	↓
	Voltage	PV Rating	↑↓↓	↑↓↓
		PPL	↑↓↓	↑

Table A1. Technical data of the network under consideration.

Distribution Transformer: 100 kVA, 50 Hz, Dyn-type, Z = 5%
MVF: 11 kV, 2 km, ACSR 50 mm^2 bare conductor, three-phase 3-wire system R = 2.16 Ω/km, X = 2.85 Ω/km [34]
LVF: three-phase 4-wire system, 415 V L-Lrms, 400 m long, AAC 75 mm^2 bare conductor with R = 0.452 Ω/km, X = 0.27 Ω/km [34], n = 10
PV inverters: PF = 1, η =100%, $I_{max} = 1.5I_{rated}$

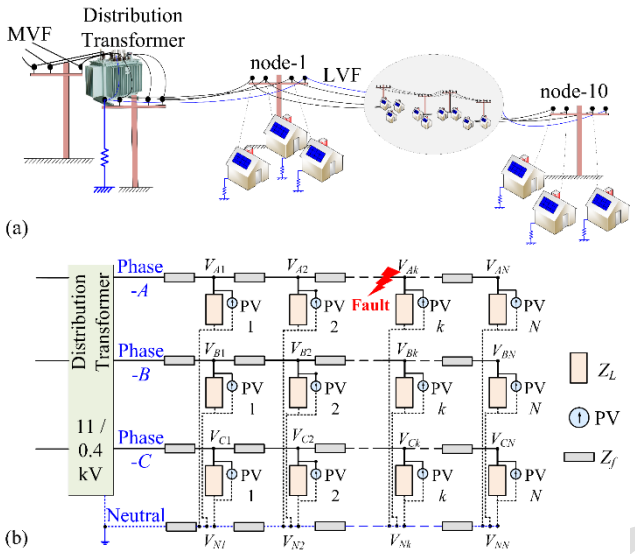

Fig. 1. Typical low voltage electrical network supplying residential customers: (a) Schematic diagram, (b) Equivalent Circuit.

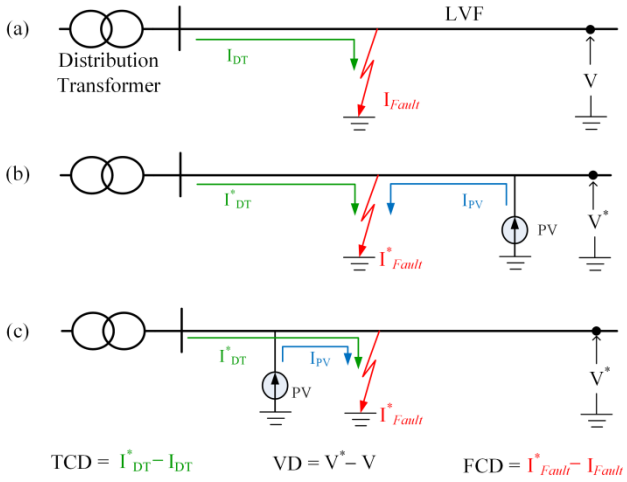

Fig. 2. Different states of PV and SCF location situations: (a) No-PV mode, (b) SCF at PV upstream, (c) SCF at PV downstream.

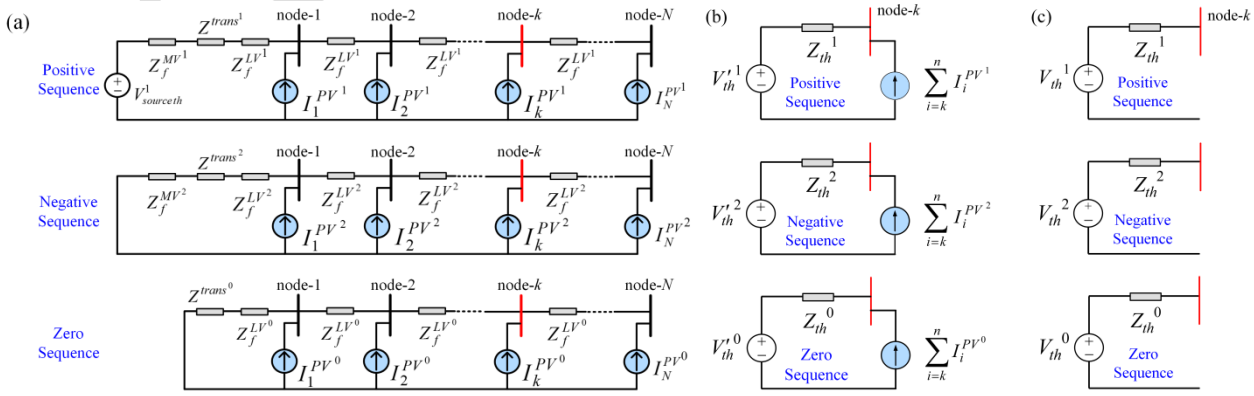

Fig. 3. (a) Sequence networks of the system of Fig. 1b for an SCF at node-k, (b) Equivalent sequence networks, (c) Simplified Thevenin equivalent of sequence networks.

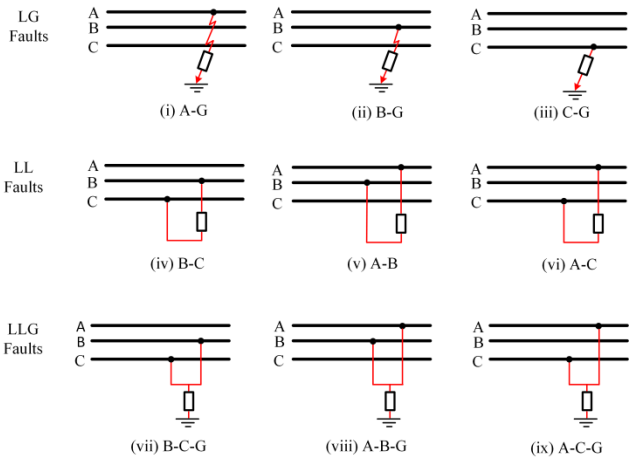

Fig. 4. Different types of faults considered in this study.

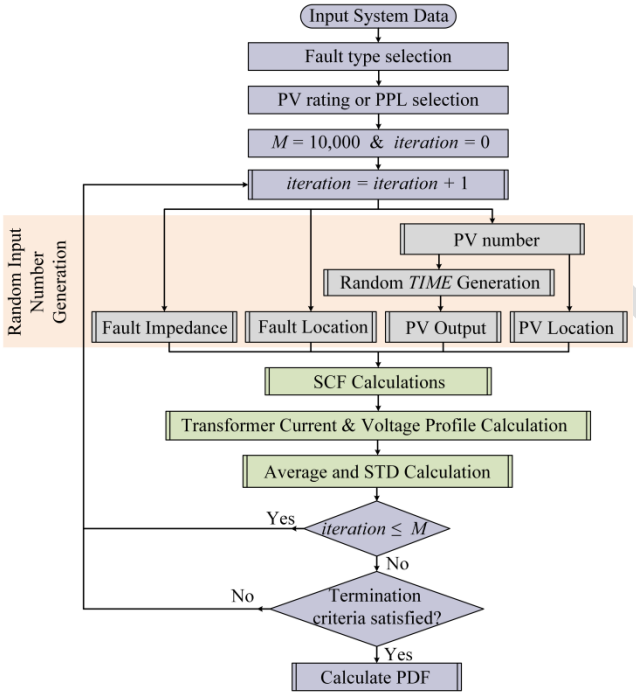

Fig. 5. Flowchart of the developed MCA.

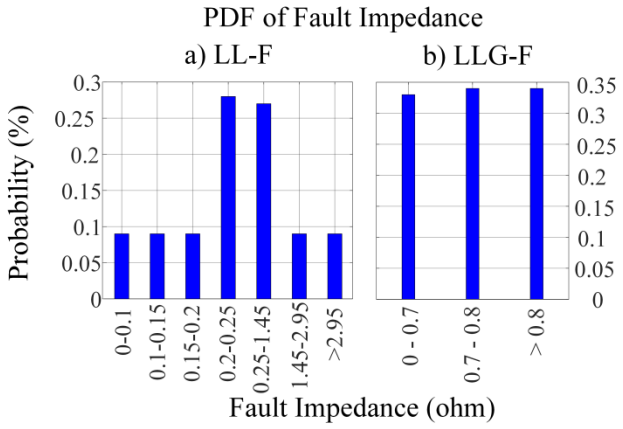

Fig. 6. Considered SCF impedance PDF for a) LL-Fs, and b) LLG-Fs.

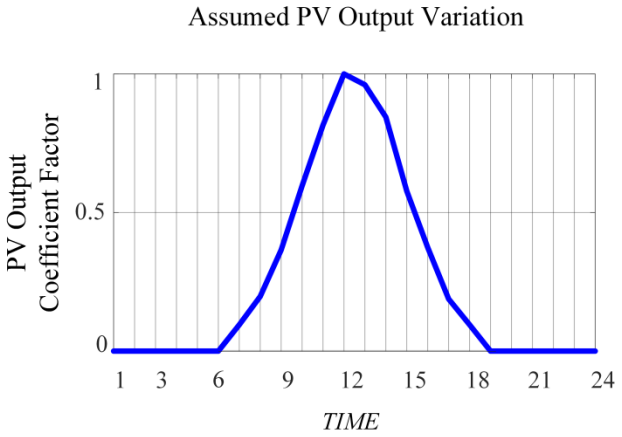

Fig. 7. Considered relation between TIME and available power from the PVs.

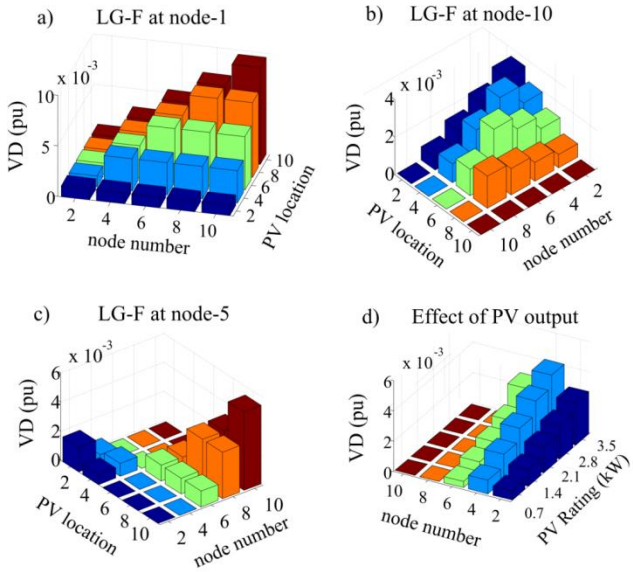

Fig. 8. Sensitivity analysis results for VD along the LVF during an LG-F.

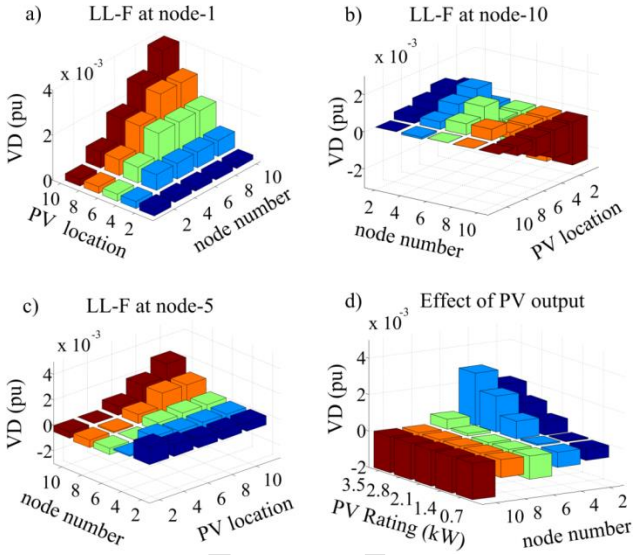

Fig. 9. Sensitivity analysis results for VD along the LVF during an LL-F.

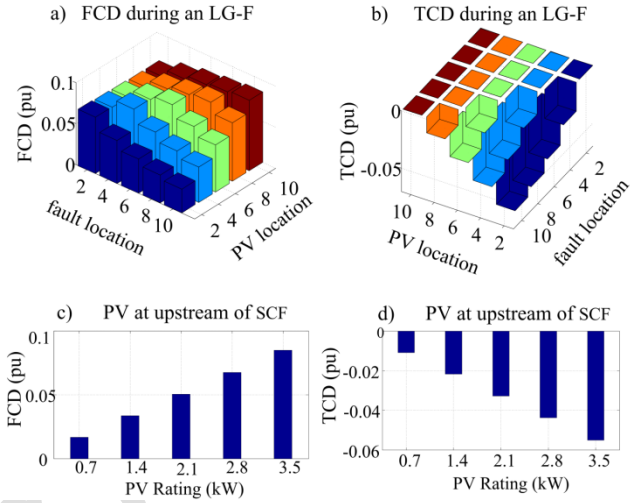

Fig. 10. Sensitivity analysis results for FCD and TCD during an LG-F.

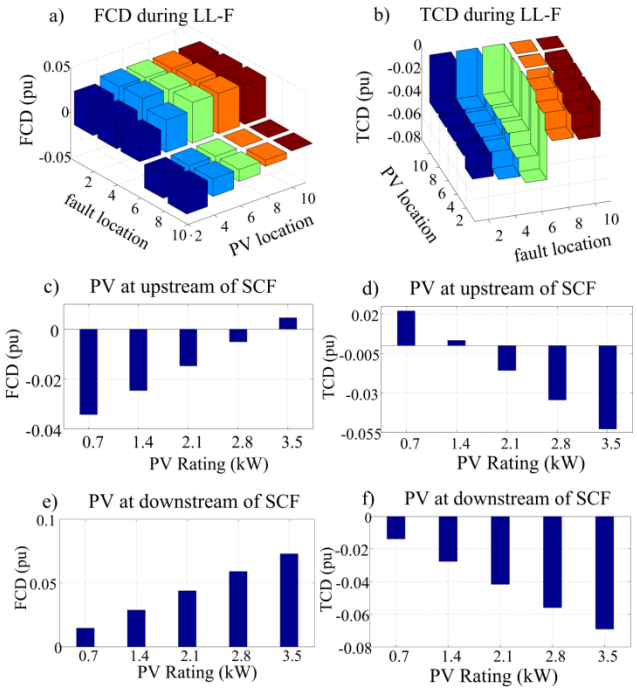

Fig. 11. Sensitivity analysis results for FCD and TCD during an LL-F.

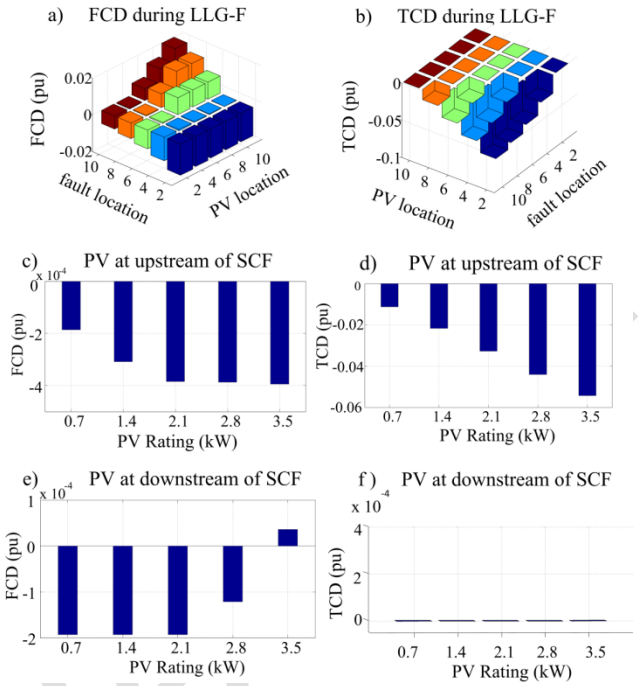

Fig. 12. Sensitivity analysis results for FCD and TCD during an LLG-F.